Neutral self-defects in a silica model: A first-principles study

L. Martin-Samos,* Y. Limoge, J.-P. Crocombette, and G. Roma
Service de Recherche en Métallurgie Physique, CEA-Saclay, 91191 Gif-sur-Yvette, France

N. Richard
CEA-DIF, Bruyère-le-Châtel, France

E. Anglada
Departamento de Fisica de la Materia Condensada, Universidad Autonoma de Madrid, Madrid, Spain

E. Artacho
Department of Earth Sciences, University of Cambridge, Cambridge, United Kingdom
(Received 11 May 2004; revised manuscript received 18 October 2004; published 28 January 2005)

We present a statistical study of silicon and oxygen neutral defects in a silica glass model. This work is performed following two complementary approaches: first-principles calculations and empirical potential molecular dynamics. We show that the defect formation energies and structures are distributed and that the energy distributions are correlated with the local stress before the defect formation. Combining defect energies calculated from first principles and local stresses from empirical potential calculations in undefected silica, we are able to predict the formation energy distributions in larger systems, the size of which precludes the use of *ab initio* methods. Using the resulting prediction we will show that the cell size used in our modeling contains all the formation energy fluctuations needed to describe a real glass.

DOI: 10.1103/PhysRevB.71.014116 PACS number(s): 66.30.Hs, 66.30.Lw, 82.20.Pm

I. INTRODUCTION

Silicate-based compounds are common materials in a variety of scientific and technological fields. One of the important questions, still open, is their long-term evolution under aging factors. The diffusion mechanisms are responsible for this long-time behavior. As silicate-based compounds are complex systems, and also as the involved time scale may extend over thousand of years, the experiments are complicated to analyze and in many cases impossible to perform without accelerated aging. In this case, the interpretation of the accelerated experiments, as well as their transposition to the actual problems, rely on the modeling of the aging phenomenon. In this context, numerical simulation appears as a powerful tool for the understanding of the defect properties and the diffusion processes, which allows then, in a multiscale simulation scheme, to understand the long-time behavior. In particular, first-principles calculations, the direct application domain of which is restricted to short times and small sizes, open up the possibility to describe the primary diffusion mechanisms.

This work focuses on a model of amorphous SiO_2, chosen as the simplest silicate-based material. It presents a first-principles study on the neutral self-defects, which are the defects coming from those chemical species present in the material. A first and partial account of this work has been already given.[1] Following previous studies performed in SiO_2 crystalline phases[2–8] and in the amorphous one,[9,10] we will focus on vacancies and intrinsic interstitials. It is known that under high enough oxygen partial pressure the main diffusion mechanism is mediated by molecular oxygen.[11–13] But, at lower pressures or under irradiation, as in nuclear glasses or in microelectronic devices, a complete knowledge of defects and their evolution is needed. The reason for beginning by studying neutral defects is twofold. First it is difficult to detect experimentally the structures and concentrations of neutral defects, which lack an electric or magnetic signature. Then, the estimation of their contribution to the diffusion and their role as precursor of other defect types has still to be clarified. Second, a recent work[14,15] on self-defects in α-quartz has shown that in pure quartz, due to the value of the electronic chemical potential, the charged defects should not contribute too significantly to the diffusion, at least in the range of usual experimental conditions. Of course these results obtained for quartz cannot be transposed directly to silica glass without an analogous study for charged defects. This will be the aim of a further publication.

The main difficulties in a numerical study of defects in an ionocovalent glass are closely related to the disorder and to the nature of the bonds implied in the defect structures. The first difficulty comes from the generation of the glass model itself. Indeed, as the glass properties depend on the quench rate and on the subsequent annealing time, it is important to quench then the melt at the slowest rate possible, in order to have a glass model close to the actual structure of a silica glass. Using *ab initio* methods the quench rate remains in excess of 10^{15}K/s, but within empirical potential molecular dynamics (EPMD) the rate can be as low as 10^{11}K/s, closer to the experimental one of 10^{5}K/s. On the other hand, even if the glassy state without defects is well described with empirical potentials, we expect that the available empirical models are completely unable to describe properly the homopolar bonds frequently involved in defect formation in SiO_2.[2–13] The third difficulty comes from the need of a comprehensive study on a large set of defect sites. As in a glass all the defect sites are nonequivalent, the properties deduced

 ©2005 The American Physical Society

from the calculations are strongly dependent on the completeness of the considered population. Nothing is known *a priori* about the minimal size of the population which will represent the average and fluctuations of the property under study in a real size glass. We choose an *ab initio* technique where the wave functions are projected onto a localized pseudo–atomic orbitals (LCAO) basis. In most cases it is possible with a relatively reduced number of basis vectors to have an accurate description of ground states. The reduced number of basis vectors results, of course, in a significant gain in computational time. But the results have to be validated by another *ab initio* approach, without the uncertainity of the basis, to ensure the consistence of the calculations. Indeed, the degree of completeness of the LCAO basis set that is chosen is not known *a priori*.

Our initial glass configuration was obtained by quenching from a melt prepared using molecular dynamics with an empirical interaction model (EPMD) with fixed charges. The *ab initio* calculations were performed using the SIESTA first-principles code[16,17] based on density functional theory (DFT) within the local density approximation (LDA) and LCAO basis set.

In the first part of the paper we present the numerical methods used as well as the main definitions. Then, in order to provide a check for our SIESTA calculations, we show a comparison between results obtained with three first-principles codes (SIESTA, PWSCF, VASP). We next present our results obtained with the SIESTA code for defects in a 108-atom silica model. As expected, at variance with SiO_2 crystalline phases, the defect structures and formation energies are noticeably scattered. The distribution is due to the structural disorder which induces the nonequivalence of defect sites. We discuss how the formation energy dispersion is related mainly to local properties in the case of oxygen defects and to medium range properties in the case of silicon defects. In this context, we show that the origin of the formation energy distribution stems from the local stress fluctuations. Combining the formation energies calculated by first principles and EPMD local stress calculations, one can construct a simple model allowing one to extrapolate the formation energies to larger systems. We then apply this model to amorphous supercells containing 192 and 648 atoms, and we prove that a 108-atom silica glass model is able to represent correctly the defect formation energies and defect formation energy fluctuations.

II. GENERATION OF THE INITIAL AMORPHOUS MODEL

The generation procedure is done in two steps. In the first step a well relaxed amorphous structure is generated by melting and quenching a SiO_2 crystalline polymorph using EPMD. In the second one the resulting amorphous model is relaxed by first principles using a conjugate gradient method. This two-step procedure is needed to obtain amorphous structures at a low CPU time cost (EPMD) and a realistic description of the binding, thanks to the first-principles account of the electronic contribution. An earlier work[18] has shown that the first-principles relaxation results in a small variation of the atomic positions, which means that the EPMD structure and the first-principles structure are really close to each other.

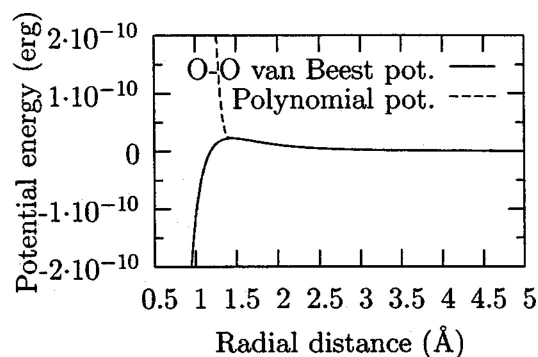

FIG. 1. O-O BKS potential and the polynomial repulsive potential.

A. Optimized quench within the EPMD approach

The annealing steps by molecular dynamics were performed at constant number of particles N, constant volume V, and constant temperature T, the so called NVT ensemble of molecular dynamics. The temperature is maintained constant by rescaling the particle velocities periodically, in order to get the required kinetic energy in the standard way. The structural relaxation were obtained using a damped dynamics on cell variables.

The van Beest–Kramer–van Santen[19] (BKS) potential, which is known to reproduce well the structural and vibrational properties of silica at low temperatures, is chosen as the empirical interaction model. However, at short distances the BKS potential diverges attractively, as shown in Fig. 1, precluding its use in its original form for molecular dynamics at high temperature. To avoid this unphysical divergence it is necessary to add a hard repulsive part (RP) acting only at shorter distances. This treatment is a standard procedure.[18,20] But, with this arbitrary addition, one has to check carefully that the amorphous structures obtained are independent of it. At high temperatures, where the atoms can be close enough to feel the repulsive part, the structures are dependent on the detailed form that is used. After the quench, the system may keep a memory of its high-temperature behavior. It is, then, necessary to control that we can define an optimized quench procedure (see below), which allows us to recover a structure free of artifacts due to this repulsive potential. We choose the same polynomial form [see Eq. (1)] for the hard repulsive part (V_{RP}), of all the atomic pairs (Si-Si, Si-O, and O-O):

$$V_{RP}(x) = G(x - x_0)^4. \tag{1}$$

The total potential energy is then

$$V_{tot}(x) = \begin{cases} V_{RP}(x) & \text{for } x \leq x_0, \\ V_{BKS}(x) & \text{for } x > x_0, \end{cases} \tag{2}$$

$$\tag{3}$$

where $V_{BKS} = q_i q_j e2/r_{ij} + A_{ij} e^{-B_{ij} r_{ij}} - C_{ij}/r_{ij}^6$ is the BKS potential.

Two parameters are necessary to adjust the hard repulsive potential: x_0 and G. The branching point x_0 is chosen as the local maximum of the BKS potential (see Fig. 1). With this choice, the temperature where the atoms no longer explore the region governed by the repulsive part is the highest possible.

The optimized quench procedure proceeds then as follows.

(1) Melting of a crystalline SiO_2 polymorph (β-crystobalite) and annealing the liquid at 7000 K.

(2) Quenching from the melt at a rate of 2.3×10^{14}K/s down to 3000 K.

(3) Annealing in the *NVT* ensemble at 3000 K until a stationary regime is obtained.

(4) Quenching at a rate of 2.3×10^{14}K/s down to 300 K.

(5) Annealing in the *NVT* ensemble at 300 K until the convergence of the mean local stress is reached.

(6) Fast quench down to 0 K at zero external pressure.

We emphasize the importance of step 3, which is the one that grants that the resulting glass is independent of the choice of the repulsive part. Indeed, 3000 K is the temperature where the atoms do not have enough kinetic energy to explore the region governed by the repulsive part, but still can diffuse far enough to wipe out this influence accumulated during steps 1 and 2. To check this, we choose to work on a 648-atom supercell in order to compare the structural properties (pair correlation functions, angles distributions, ring statistics, etc.) with earlier EPMD calculations.[20–22] In order to follow the structural evolutions we plot the instantaneous ring[47] distribution in the sense of King.[23] This particular ring statistics focuses on the smallest closed path starting and ending at a particular silicon atom.

Let us recall that the defect-free SiO_2 glass may be considered as a well connected network built on SiO_4 tetrahedra and that ring statistics is a powerful tool to describe the connectivity of amorphous networks. The choice of ring statistics as a tracer of the structural convergence is motivated by the fact that it shows the topological changes related to the break of Si-O bonds, free of the bond stretching signal, in contrast to the instantaneous pair correlation function and related short-range quantities. Another advantage is that ring statistics is a more discriminant factor than pair correlation functions. The local order, represented by the first peak in pair correlation functions, in silica is always well defined and thus cannot be used as discriminant. To extract information about the medium range order it is necessary to look at the shape and position of the rest of the peaks. However, it is not possible, with the information given by these peaks to distinguish beetwen network distortions or network connectivity changes because they only give the distance distribution with rotational symmetry. The evolution of these topological changes is precisely what we are looking for. Many different ways to count the rings exist in the literature,[23–28] but whatever definition is used, having the same ring statistics is a necessary condition to have the same structure.

We start with two β-crystobalite cristals of 648 atoms, systems A and B. We perform steps 1 and 2 for two different repulsive potential intensities $G_1=10^{25}$ erg/cm^4 for system A and $G_2=10^{23}$ erg/cm^4 for system B. In the third step we switch the intensities, in order to relax the system A when using G_2 and the system B when using G_1. If both systems reach the same statistical equilibrium structure after some relaxation time, then the independence of the choice of a repulsive potential form is recovered. After approximatively 1 750 000 time steps, both systems (A and B) reach the same time average ring statistics, as show in Fig. 2 where the evolution for three-membered and five-membered[48] rings is plotted during the anneal at 3000 K. This convergence is also observed for the other ring sizes. Thus independence from the repulsive potential form is proved.

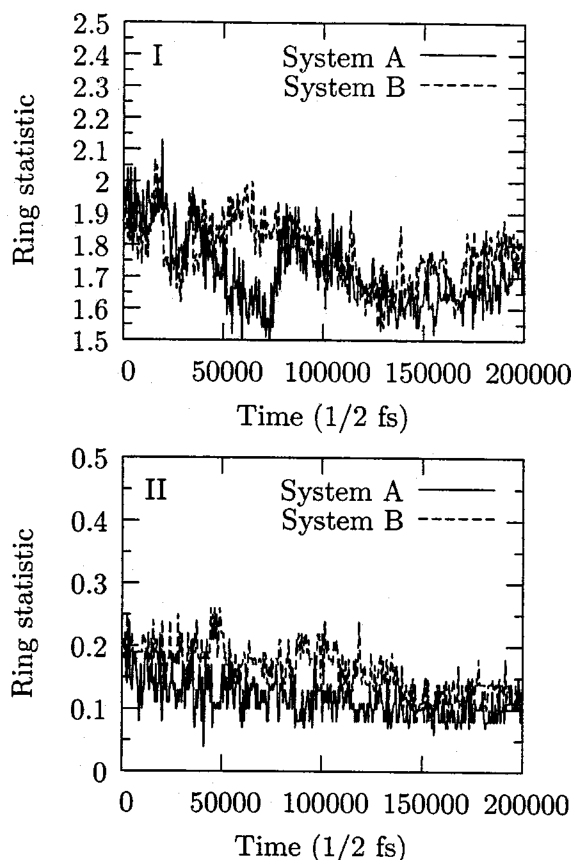

FIG. 2. Five-membered (I) and three-membered (II) ring statistics time evolution during the anneal at 3000 K.

The procedure is quite insensitive to the choice of the melting temperature in step 1, the quench rate in steps 2 and 4, and the relaxation temperature in step 5. Conversely, a long relaxation at room temperature is necessary to ensure that mean local stress convergence is achieved before the last step (step 6). The silica model built on this six-step quench procedure exhibits a structure very close to the experimental one, independently of which hard repulsive potential is chosen.

B. Structure of the glass models generated by the optimized quench procedure

Using the procedure described above (Sec. II A) we generate three amorphous models of different size: 108, 192, and 648 atoms. The 108-atom model is used for the complete first-principles study of point defects. In terms of local prop-

TABLE I. Mean angles and full width at half maximum (FWHM) in the EPMD amorphous models and mean angles in the silica glass.

	108 atoms	192 atoms	648 atoms	Experiment
Si-Si-Si	107.7°	107.8°	107.5°	
Si-Si-O	81.1°	85.8°	83.7°	
O-Si-O	109.0°	109.3°	109.2°	109.4° (Ref. 31)–109.7° (Ref. 32)
FWHM	13°	15°	16°	
Si-O-Si	153.5°	148.4°	148.9°	144°–152° (Ref. 32)
FWHM	42°	27°	33°	
O-O-O	96.1°	97.2°	97.0°	
O-O-Si	82.1°	87.5°	84.9°	

erties like mean first-neighbor distances, even with a relatively small silica model, the agreement between the model and the experimental data remains very good (as shown in Tables I and II). In other words, the size dependence is negligible. But this is not the case, for instance, for ring statistics, which describes medium range properties. The highest-order rings decrease with increasing size of the system while the five-membered rings per Si center increase, and the three-, four-, and six-membered ring populations are almost constant (see Table III). The size of the system, due to the periodic boundary conditios, fixes the highest-order ring. Five-membered rings are energetically more favorable[29] than three- or four-membered rings. The six-membered ring statistic seems to be almost constant ($\approx$two six-membered rings per Si center) in EPMD silica models.[20,22,30] As we do not know *a priori* the range of the defect formation energy, we need larger-size silica models to perform a size dependency study. The 192-atom model is, then, needed to check whether the average and fluctuations of the defect formation energy is well represented or not by the 108-atom model. Some *ab initio* calculations (oxygen vacancy formation energy) have been performed for this model. Finally, the 648-atom model which will be treated only classically, is used to extrapolate the defect formation energies.

Looking at Tables I–III, we conclude that the optimized quench procedure gives well connected amorphous networks, without two-membered rings (edge sharing tetrahedra) even for relatively large (648 atoms) system size. The BKS potential, combined with the optimized quench procedure, predicts the structure commonly postulated for ideal amorphous silica.

TABLE II. Mean first-neighbor distances and full width at half maximum (FWHM) in the EPMD silica models and in the silica glass.

	108 atoms	192 atoms	648 atoms	Experiment (Ref. 33)
d(Si–Si)(Å)	3.16	3.07	3.16	3.12
FWHM (Å)	0.28	0.21	0.23	
d(Si–O)(Å)	1.60	1.61	1.60	1.62
FWHM (Å)	0.07	0.08	0.06	
d(O–O)(Å)	2.61	2.76	2.58	2.65
FWHM (Å)	22	25	24	

C. The first-principles relaxation

For the first-principles part, we choose to use the SIESTA code based on DFT-LDA, with Martin-Troullier pseudopotentials to describe the core-valence electronic interaction. SIESTA uses localized pseudo–atomic orbitals as a wave function basis. The atomic positions and cell parameters are relaxed using the conjugate gradient method. Given the large supercell size (108 and 192 atoms), the Brillouin zone is sampled at the Γ point only. The use of SIESTA is motivated by the fact that with a reduced basis set it is possible in some cases to give accurate results at low computational effort. Naturally, the search for reducing the computational time is due to the need for a statistical study. As in a glass all the defect sites are nonequivalent, one expects to have formation energy distributions and also a distribution of structural parameters. In that context, it is important to study a large number of defect sites. The basis set used is double-zeta polarized *sp* orbitals for silicon and oxygen (basis optimization done by Anglada *et al.*[34]).

To validate the accuracy of the basis set chosen, we have compared the SIESTA results to two other first-principles schemes, where the error due to the noncompleteness of the basis set can be controlled. We used a β version[35] of PWSCF

TABLE III. Ring statistics in the sense of King (Ref. 23) of the EPMD silica models.

Ring order	108 atoms	192 atoms	648 atoms
2	0	0	0
3	0.167	0.047	0.069
4	0.556	0.500	0.537
5	3.194	2.297	1.866
6	2.028	2.391	1.995
7	0.056	0.750	1.208
8	0	0.016	0.319
9	0	0	0.046
10	0	0	0

TABLE IV. Density of the first-principles amorphous models.

	SIESTA	PWSCF	VASP
Density (g/cm^3)	2.19	2.18	2.23

within the LDA, with norm-conserving pseudopotentials and an energy cutoff of 80 Ry. We have also performed calculations with VASP (Refs. 36–38) within the projector augmented wave (PAW) approach,[38] using an energy cutoff of 500 eV (~37 Ry). The atomic positions and cell parameters are relaxed by the conjugate gradient method. In the VASP calculations, in the case of defective silica, the atomic positions are relaxed at constant volume.

As shown in Tables IV–VI, the densities and structures of the silica models after the first-principles relaxation are very close for all the methods used. Of course these results only show that the basis is complete enough to give an accurate description of the glass structure. In Sec. IV we compare the three codes in the context of defect state calculations.

III. THE DEFECT STATE CALCULATIONS

The ground state energy of the system with one defect is obtained by adding (interstitials) or removing (vacancies) an atom and relaxing the resulting structure, atomic positions, and cell parameters by first principles. We perform ground state energy calculations for all of the 72 oxygen vacancy and interstitial sites, for all of the 36 silicon vacancy sites, and for 84 silicon interstitial sites, using the same methods and parameters as in the first-principles relaxation of the nondefective silica (Sec. II C). In the case of interstitial silicon the starting points of the extra silicon atom were chosen at random among the centers of the rings of the structure. 120 such starting points have been selected, giving rise to 84 stable, or metastable, different configurations of the defect.

For the formation energy calculations we suppose that SiO_2 is in equilibrium with the O_2 molecular gas, according to the following reactions and equations:

Oxygen vacancy:

$$SiO_2 - \tfrac{1}{2}O_2 \rightleftharpoons (SiO_2)^{V^O},$$

$$E_f^{V^O} = E_{\text{supercell}}^{V^O} - \left(E_{\text{supercell}} - \tfrac{1}{2}E(O_2)\right).$$

TABLE V. Mean angles in the first-principles amorphous models.

	SIESTA	PWSCF	VASP
Si-Si-Si	107.8°	108.6°	108.5°
Si-Si-O	86.2°	86.0°	86.0°
O-Si-O	109.0°	109.4°	109.4°
Si-O-Si	142.5°	145.1°	144.9°
O-O-O	98.4°	98.7°	98.4°
O-O-Si	87.0°	86.8°	86.8°

TABLE VI. Mean first-neighbor distances in the first-principles amorphous models.

	SIESTA	PWSCF	VASP
d(Si-Si)(Å)	3.07	3.08	3.12
d(Si-O)(Å)	1.63	1.62	1.61
d(O-O)(Å)	2.75	2.73	2.63

Oxygen interstitial:

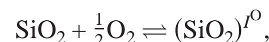

$$SiO_2 + \tfrac{1}{2}O_2 \rightleftharpoons (SiO_2)^{I^O},$$

$$E_f^{I^O} = E_{\text{supercell}}^{I^O} - \left(E_{\text{supercell}} + \tfrac{1}{2}E(O_2)\right).$$

Silicon vacancy:

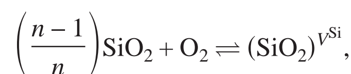

$$\left(\frac{n-1}{n}\right)SiO_2 + O_2 \rightleftharpoons (SiO_2)^{V^{Si}},$$

$$E_f^{V^{Si}} = E_{\text{supercell}}^{V^{Si}} - \left[\left(\frac{n-1}{n}\right)E_{\text{supercell}} + E(O_2)\right].$$

Silicon interstitial:

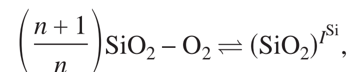

$$\left(\frac{n+1}{n}\right)SiO_2 - O_2 \rightleftharpoons (SiO_2)^{I^{Si}},$$

$$E_f^{I^{Si}} = E_{\text{supercell}}^{I^{Si}} - \left[\left(\frac{n+1}{n}\right)E_{\text{supercell}} - E(O_2)\right].$$

Here E_f is the defect formation energy, $E_{\text{supercell}}$ is the energy of a perfect silica supercell containing n tetrahedra, and $E_{\text{supercell}}^{V \text{ or } I}$ is the energy of the silica supercell with a point defect, containing now $n-1$ or $n+1$ silicon/oxygen atoms, depending on the defect being a vacancy or an interstitial. The ground state energy of the oxygen molecule is calculated with spin polarization.

IV. VALIDATION OF THE BASIS SET

In order to confirm that our LCAO basis set is reliable also for the defect properties, we have calculated defect formation energies in α-quartz as well as a few defects, three for each of silicon and oxygen, on the same sites of the glass model, with both approaches, the atomic and plane wave bases.

In the case of the oxygen vacancy, there is a good agreement beetwen SIESTA and PWSCF. Conversely, the formation energies given by VASP are systematically higher by 0.2 eV (see Tables VII and VIII and Fig. 3). We can, *a priori*, attribute this systematic difference to two causes: the lack of volume relaxation in our VASP calculations or the different first-principles approaches, PAW in the case of VASP and norm-conserving pseudopotentials in the cases of SIESTA and PWSCF, resulting in a different description of Si-O and Si-Si bonds. Some calculations at constant hydrostatic pressure with VASP have shown that the major contribution to this 0.2

TABLE VII. Defect formation energies, in eV, in a 72-atom α-quartz supercell, where *V*O and *I*O refer, respectively, to oxygen vacancy and oxygen interstitial, and *V*Si and *I*Si to silicon vacancy and silicon interstitial.

Defect type	SIESTA	PWSCF	VASP
*V*O	5.58, 5.59 (108 atoms)	5.58	5.80
*I*O	1.92, 1.80 (108 atoms)	1.84	
*V*Si	4.79	4.51	4.58
*I*Si	13.67	13.78	14.34

eV difference should come from the second cause, the description of the Si-O and Si-Si bonds. Indeed, the cohesive energy of bulk silicon is lower in the VASP calculations and the formation energy of silica is higher. This means that the Si-O bond is more stable and the Si-Si bond is less stable compared to the SIESTA and PWSCF calculations. In the case of oxygen vacancies, two Si-O bonds are broken and one Si-Si bond is formed. As it is less favorable to break Si-O bonds and to form Si-Si bonds in the VASP calculations than in the SIESTA and PWSCF ones, this gives a higher formation energy of oxygen vacancies for VASP.

In a few cases for oxygen interstitials, the formation energy differences between SIESTA, PWSCF, and VASP may reach 0.5 eV. As is well established, SiO_2 displays a large number of local structural conformations, corresponding to rotations of tetrahedra (see Stoneham *et al.*[9]), which are metastable with respect to the true ground state. The different relaxation methods, i.e., different Hamiltonian and different conjugate gradient algorithms, will stop the system in different metastable positions. This is clearly observable in Fig. 4, where a few points, in one or the other code, escape the one-to-one linear relation. For instance, performing constrained relaxations around the silicon-silicon axis for one oxygen interstitial displaying a formation energy of 1.38 eV, we found a metastable minimum 0.91 eV higher.

For silicon vacancies, there is a good agreement between the three codes (Tables VII and IX). In silica, silicon vacancies may exhibit three different equilibrium structures, all involving O-O bonds. The comparison between SIESTA and VASP (Table IX) for these three structures shows that the LCAO basis reproduces the VASP results.

For silicon interstitials, where a Si-Si bond has to be formed, we find, as well as in oxygen vacancies, a systematic shift, of about 0.6 eV, between VASP formation energies and the two other codes (Tables VII and IX). Clearly, the Si-Si bond in the VASP calculations is less favorable than in SIESTA and PWSCF calculations. The origin of this underbinding of silicon is certainly not in the PAW approach *per se*, but more likely lies in the manner the projectors have been implemented in VASP. To correct this peculiarity was not in the scope of this work, as soon as the main goal to validate the SIESTA basis was reached.

TABLE VIII. Oxygen formation energies, in eV, in a 108-atom glass supercell; same notation as in Table VII.

Defect type	SIESTA	PWSCF	VASP
*V*O	4.70	4.68	4.92
*V*O	5.70	5.73	5.95
*V*O	5.94	6.00	6.20
*I*O	1.62	1.86	1.75
*I*O	1.14	1.54	1.19
*I*O	1.31	1.25	1.31

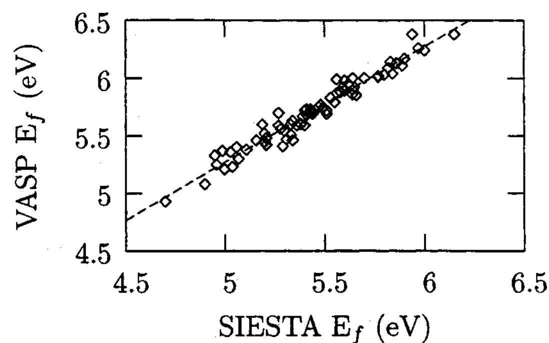

FIG. 3. Formation energies of the oxygen vacancies in a 108-atom silica glass, VASP versus SIESTA results. Fit parameters: slope $=1.005$, intercept$=0.25$ eV, correlation coefficient$=0.98$.

The energy discrepancies due to the relative noncompleteness of the localized basis set chosen for the SIESTA calculations are smaller than the energy discrepancies due to changes in first-principles scheme coming from small differences in the description of bonds. All those comparative calculations show that the basis set chosen is complete enough to give accurate results in the study of intrinsic neutral defects in the silica. The rest of the study has been therefore performed only with the SIESTA code.

V. NEUTRAL SELF-DEFECTS IN A 108-ATOM SILICA GLASS

A. Oxygen defects

The structures of the neutral oxygen vacancies and interstitials are found to be a Si-Si crystalline siliconlike bond and a Si-O-O-Si peroxy bridge, respectively, as in α-quartz.[8] The bond length and formation energies are distributed. Fig-

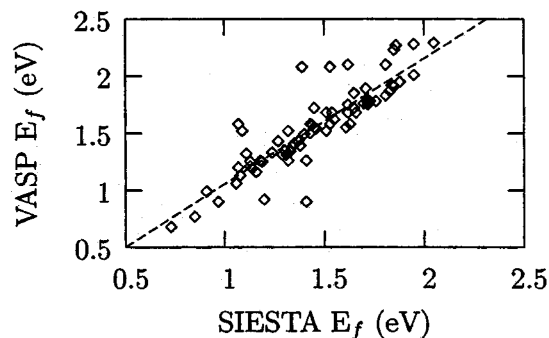

FIG. 4. Formation energies of the oxygen interstitials in a 108-atom silica glass, VASP versus SIESTA. Fit parameters: slope$=1.028$, intercept$=0.048$ eV, correlation coefficient$=0.85$.

TABLE IX. Silicon formation energies, in eV, in a 108-atom glass supercell; same notation as in Table VII.

Defect type	SIESTA (eV)	VASP (eV)
*V*Si	2.55	2.57
*V*Si	3.95	3.88
*V*Si	5.68	5.69
*I*Si	12.03	12.63
*I*Si	11.56	12.47
*I*Si	12.54	12.84

ures 5 and 6 show the formation energies, which follow Gaussian-like distributions.

The mean oxygen vacancy formation energy and standard deviation are 5.44 eV and 0.3 eV, respectively. The mean formation energy of the Gaussian fit is 5.52 eV with a standard deviation of 0.3 eV. The Si-Si bond length spans from 2.2 to 2.6 Å, with an average value of 2.36 Å. The mean formation volume is −25.0 Å^3.

The mean oxygen interstitial formation energy and standard deviation are 1.46 eV and 0.4 eV, respectively. The mean formation energy of the Gaussian fit is 1.60 eV with a standard deviation of 0.4 eV. The O-O bond length spans the 1.3 to 1.5 Å range, with an average value of 1.46 Å. The mean formation volume is 6.6 Å^3.

In silica, the average formation energy for the oxygen defects is lower by 0.15 and 0.34 eV for the vacancies and interstitials, respectively, than in α-quartz. The average Frenkel pair formation energy is then 0.5 eV smaller than in α-quartz. However, these results gives a crucial information. Even if the medium- and long-range structure between quartz and silica glass is completely different, the structure and the formation energy of oxygen defects are very close. This can be understood only if the oxygen defect depends mainly on the local order. Indeed, the local first-neighbor order in silica glass is very well defined and very close to the crystalline tetrahedral arrangement, giving rise to high intensities of the pair correlation function first peak. In this picture, the distributions come from small deviations from the local perfect order, as we shall see below.

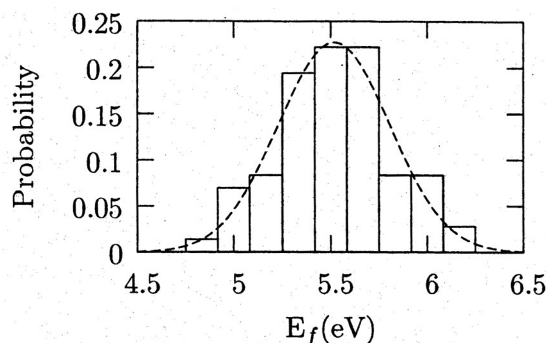

FIG. 5. Formation energy distribution of the oxygen vacancy in a 108-atom silica glass. Parameters of the Gaussian fit: mean value=5.52 eV, standard deviation=0.3 eV

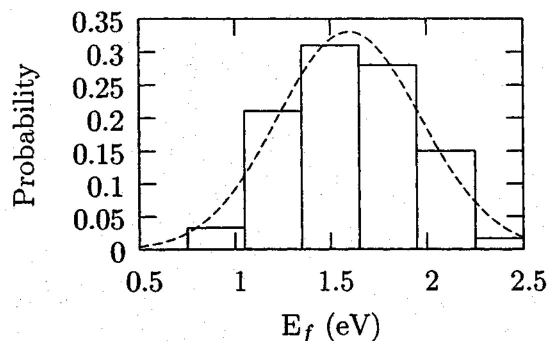

FIG. 6. Formation energy distribution of intrinsic-oxygen interstitial in a 108-atom silica glass. Parameters of the Gaussian fit: mean value=1.60 eV, standard deviation=0.4 eV.

B. Silicon defects

The neutral silicon defects have a more complicated behavior than the neutral oxygen defects, and display many different equilibrium structures as shown in Table X, where only atoms with coordination anomalies and their first neighbors have been represented. In the case of the silicon vacancies, due to the relatively limited sampling (36 silicon vacancies) it is difficult to give a precise general behavior for the formation energies. We observe three different structures: an ozonyl bridge, a double peroxy bridge, and a single peroxy bridge plus two nonbridging oxygens. The double peroxy bridge corresponds to the structure of the neutral silicon vacancy in α-quartz. When it is formed, the ozonyl bridge is the most stable structure with the smallest average formation energy (2.24 eV). The mean formation energy for all structures is 3.80 eV, 0.7 eV smaller than in α-quartz,[8,14,15] and the mean formation volume is −1.88 Å^3.

In the case of silicon interstitials, the results are summarized in Table X, where we give the various structures and mean formation energies as well as the probability of finding a defect site with a particular structure (see also Figs. 7 and 8). This probability is obtained from the number of defect introduction sites giving the specific defect structure divided by the total number of introduction sites. In the case of vacancies this last number is simply the number of tetrahedra; for interstitials it is the number of large cavities in the silica model used as introduction points for the extra silicon and giving rise to different defects (i.e., 84 sites as said above). By far the most probable structure is the Si-Si-O link (I^1), where the silicon interstitial is inserted beetwen a Si-O bond, as in α-quartz. Similarly to the oxygen interstitial case, local minima exist around the Si-O defect axis. The energy differences between them may reach 1 eV. More complicated and compact defect structures are also found; one of the most interesting is the double-oxygen-vacancy-like structure (I^2). The silicon interstitial is inserted on a Si-O bond and then the silicon atom bonds to a neighboring silicon, stealing one of its oxygens. This structure has the smallest formation energy, 11.52 eV on average, close to the formation energy of a bivacancy. Indeed, using the mean formation energy of an oxygen vacancy, resulting from the Gaussian fit of Fig. 5, in Sec. V A, and neglecting the contribution of the interaction between vacancies, the average formation energy of a diva-

TABLE X. Symbolic representation [silicon atoms (dark gray) and oxygen atom (light gray)] of the structure of silicon defects, where only atoms with coordination changes and their first neighborhood have been plotted; average formation energy ($\langle E_f \rangle$); and structure probability of the silicon vacancies (V) and interstitials (I).

Defect type	Structure	$\langle E_f \rangle$(eV)	Probability (%)
V^1		5.86	39 %
V^2		3.30	53 %
V^3		2.24	8 %
I^1		12.54	83 %
I^2		11.52	5 %
I^3	, etc	13.37	12 %

cancy amounts to 11.04 eV. In the other cases, summarized by I^3 in Table X, the inserted silicon produces a partial reconstruction in its neighborhood giving rise to three-coordinated oxygens. Their formation energies are, on average, higher than the other two cases (I^1 and I^2). The mean formation energy including all structures is 12.48 eV, 1.3 eV smaller than in α-quartz,[15] and the mean relaxation volume is -41.5 Å^3.

VI. DISCUSSION

In silica glass the medium- and long-range structures are markedly different from those in quartz and so also is the environment seen by each defect site. Conversely, the short-range structure, which means first-neighbor tetrahedra, is well defined and close to the first-neighbor tetrahedral order found in quartz or crystobalite.[6] The intrinsic oxygen defects have a single structure for each kind of defect type, the same as in α-quartz. Their formation energies are distributed according to Gaussian distributions with a mean value close to the formation energy of oxygen defects in α-quartz. Both results point to the probable fact that the major contribution to the formation energy dispersions comes from variations of local properties. The formation energy dispersion is likely to depend on small deviations from the "perfect" first-neighbor tetrahedral order. The question is then how to characterize these small deviations.

Conversely, the silicon defects show several different structures. The mean formation energies corresponding to these structures are quite distinct. This could be the signature of a medium-range order dependence, typically second-neighbor distances, ring statistics on the defect site, or similar properties. However, as the most probable structures is always the same as in α-quartz, we still expect to find a relation between formation energy and local glass structure, with nevertheless some blurring of the energy-structure relationship.

A. Origin of the formation energy dispersion

As sketched above, the formation energy dispersion should depend on local structural fluctuations of undefected

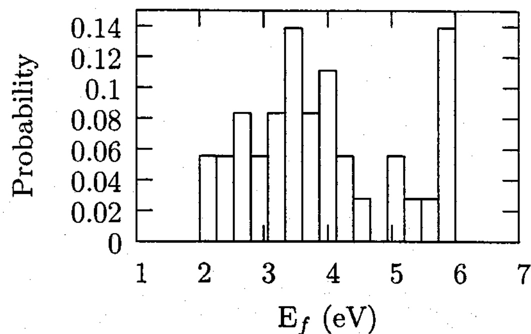

FIG. 7. Formation energy distribution of silicon vacancy in a 108-atom silica glass.

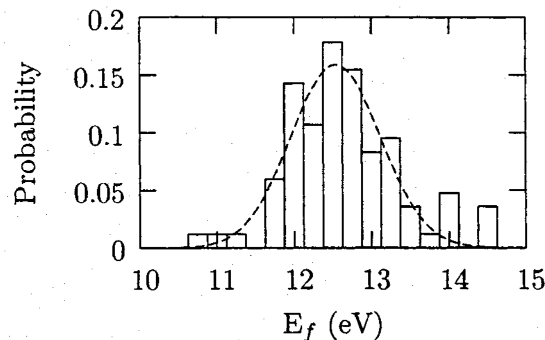

FIG. 8. Formation energy distribution of silicon self-interstitial in a 108-atom silica glass. Parameters of the Gaussian fit: mean value=5.52 eV, standard deviation=0.3 eV

silica, more likely in the case of oxygen defects than in silicon defects. We have searched for a structure dependence of the formation energies. We have investigated several structural parameters of the nondefective silica model, in particular, bond distances, Voronoi volumes, intra- and intertetrahedra angles, very strong ring statistics,[28] and the local stresses.

We have found a very clear dependence on the local stresses at the defect site before the introduction of the defect. It is possible to construct a simple model based on the Kanzaki forces and the dipole tensor,[39–41] to fully explain this behavior.

The formation energy of a defect in a uniformly deformed system under the homogeneous deformation ϵ is

$$E_f = [\phi(R_0 + s + u_{\rm ds}) + \Delta\phi(R_0 + s + u_{\rm ds})] - \phi(R_0 + s) \quad (4)$$

where ϕ is the potential energy function of the system, R_0 are the positions in the unstrained system, s is the displacement from the reference positions produced by the strain ($s = \epsilon \cdot R_0$), $u_{\rm ds}$ is the variation of the displacement due to the defect, and $\Delta\phi$ is the variation of the potential energy function of the system due to the introduction of the defect. Expanding ϕ around R_{0+s} to second order and $\Delta\phi$ to first order in the defect perturbation,

$$E_f = \left(\frac{\partial \phi(R_0 + s + u_{\rm ds})}{\partial u_{\rm ds}}\right)_{u_{\rm ds}=0} \cdot u_{\rm ds} + u_{\rm ds} \cdot \left(\frac{\partial^2 \phi(R_0 + s + u_{\rm ds})}{\partial u_{\rm ds}^2}\right)_{u_{\rm ds}=0} \cdot u_{\rm ds} + \Delta\phi(R_0 + s) + \left(\frac{\partial \Delta\phi(R_0 + s + u_{\rm ds})}{\partial u_{\rm ds}}\right)_{u_{\rm ds}=0} \cdot u_{\rm ds} + O(u_{\rm ds}^2) \quad (5)$$

where the dot product "·" means a single index contraction. Under the assumption that at $R_0 + s$ there is no net force in the system since it is in equilibrium, and applying the equilibrium condition to the system, we obtain

$$0 = u_{\rm ds} \cdot \left(\frac{\partial^2 \phi(R_0 + s + u_{\rm ds})}{\partial u_{\rm ds}^2}\right)_{u_{\rm ds}=0} + \left(\frac{\partial \Delta\phi(R_0 + s + u_{\rm ds})}{\partial u_{\rm ds}}\right)_{u{\rm ds}=0} \quad (6)$$

and then

$$u_{\rm ds} = -\left(\frac{\partial^2 \phi(R_0 + s + u_{\rm ds})}{\partial u_{\rm ds}^2}\right)^{-1}_{u_{\rm ds}=0} \cdot \left(\frac{\partial \Delta\phi(R_0 + s + u_{\rm ds})}{\partial u_{\rm ds}}\right)_{u{\rm ds}=0}, \quad (7)$$

where $[\partial \Delta\phi(R_0 + s + u_{\rm ds}) / \partial u_{\rm ds}]_{u{\rm ds}=0}$ are the forces exerted by the defect. Inserting Eq. (7) in the expansion of Eq. (4), the formation energy may be written to second order in the defect perturbation as

$$E_f = \Delta\phi(R_0 + s). \quad (8)$$

Expanding the right hand side of Eq. (8) around s, we get

$$E_f = \Delta\phi(R_0) + s \cdot \left(\frac{\partial \Delta\phi(R_0)}{\partial s}\right) = \Delta\phi(R_0) - P^H : \epsilon \quad (9)$$

where the double dot ":" means a double index contraction, and P^H is the dipolar tensor within Hardy's approximation,[39,40] defined as the tensor product of the forces exerted by the defect on the reference system ($\{R_0\}$):

$$P^H = -\left(\frac{\partial \Delta\phi(R_0 + s)}{\partial s}\right)_{s=0} \otimes R_0. \quad (10)$$

The formation energy of a defect under a homogeneous global strain is a linear function of the Hardy dipolar tensor and the strain:

$$E_f = \Delta\phi(R_0) - P^H : \epsilon. \quad (11)$$

To the same level of approximation, ϵ could be rewritten as a function of the stress tensor; then we get

$$E_f = \Delta\phi(R_0) - P^H : C^{-1} : \sigma, \quad (12)$$

where C is the elastic constant tensor and σ is the stress tensor.

In a glass, each local volume is strained in some way, with respect to the perfect tetrahedral order. To summarize, each local volume indexed by i is strained by ϵ_i. If we suppose that the dipolar tensor has a range smaller than the range of homogeneity of ϵ_i, the global strain of Eq. (11) may be replaced by the local strain ϵ_i. This local ϵ_i may be rewritten as $C^{-1} : \sigma_i$, where C is the elastic constant tensor and σ_i is the local stress tensor in the local space volume indexed by i, giving the following formation energy expression:

$$E_f^i = \Delta\phi(R_0) - P^H : C^{-1} : \sigma_i. \quad (13)$$

Equation (13) predicts a linear behavior between the formation energies and the local stress. C, as a multiplicative factor between the local strain and the local stress, may vary between each local volume, and this fact would be a source of departure from the linear behavior of Eq. (13).

The local space volume where the local stress is calculated can be chosen from the atomic scale up to the medium-range scale, but one has to be careful about its size. Indeed, if the region is larger than the range of the local stress fluctuations then the local stress will be averaged and the relevant fluctuations will be lost. We choose to characterize local stress fluctuations only on an atomic scale using the definition of atomic stress tensor proposed by Vitek and Egami,[42] based on the work of Martin and Co-workers.[43,44]

The local stress calulations are performed using the empirical interaction model. As the EPMD glass structure and the first-principles structure are very close to each other[18] (see also Secs. II B and IV), the EPMD atomic stress may be used as a measure of the local distortions. As we are interested in the origin of the formation energy dispersions, even if the absolute energy reference between EPMD and the first-principles methods is different, we expect that we get the same energy variations due to local distortions of the first-neighbor tetrahedral order.

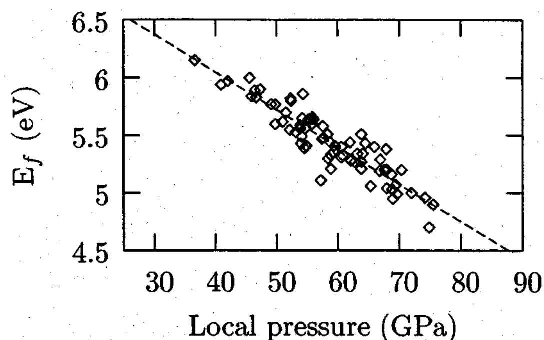

FIG. 9. Oxygen vacancy formation energies versus the initial local stress. The correlation coefficient for the linear regression is 0.92.

Within the first-order approximation in strain, and assuming pairwise interaction potentials, the atomic stress tensor is written as

$$\sigma_i^{\alpha\beta} = \frac{1}{2\Omega}\left(\frac{-2P_i^{\alpha}P_i^{\beta}}{m_i} + \sum_j^N f_{ij}^{\alpha} r_{ij}^{\beta}\right) \quad (14)$$

where r_{ij} is the relative coordinate of particles i and j, P_i is the conjugate momentum of particle i, and f_{ij} is the force. N and Ω are the total particle number and the mean atomic volume, respectively.

In the case of oxygen defects, shown in Figs. 9 and 10, we plotted the formation energy of a defect at a given site as a function of the atomic pressure before the defect creation. The agreement between the results and the model is very good. The correlation coefficients of the linear fits are 0.92 and 0.84 for the vacancies and the interstitials, respectively. Clearly, the formation energy dispersions are related to deviations from the perfect first-neighbor tetrahedral order. In the plots we have only taken into account the local pressure; if to this local pressure we add an invariant representing some local shear stress, then the dispersion in reduced. Indeed, Eq. (13) is a relation between the formation energy dispersion and the whole local stress tensor. But there still exists a residual dispersion which may come from intrinsic approximations in the model, which is only of second order in defect-induced displacements, as well as from the nonlinearity implied in the breaking and/or formation of bonds.

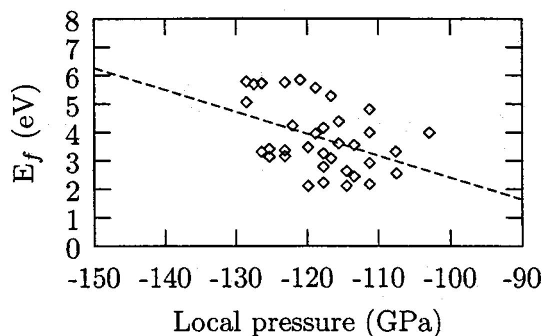

FIG. 11. Silicon vacancy formation energies versus the initial local stress.

In the case of silicon defects, the relation is also verified but with higher dispersions, as shown in Figs. 11 and 12. In the interstitial case we have used only the formation energies of silicon interstitials which belong to the I^1 group from Table X. For vacancies the dispersion is so high that only a tendency may be extracted from the relation plotted in Fig. 11. As already pointed out above, the fact that silicon defects exhibit different structures is the fingerprint that not only short-range factors are implied in the structure and formation energy variations.

B. System size convergence of the formation energy distributions

The model sketched above allows us to extrapolate the behavior observed on small systems to larger ones. To validate this idea we have built, with the same procedure described in Sec. II A, a silica model including 192 atoms and calculated the formation energy of oxygen vacancies on 28 vacancy sites. As shown in Fig. 13 the models for the 108-atom system and the 192-atom system exhibit the same slope and y intercept. The extrapolation of the 192-atom linear regression to the complete vacancy sites (128 vacancy sites) gives an average formation energy of 5.44 eV with a stan-

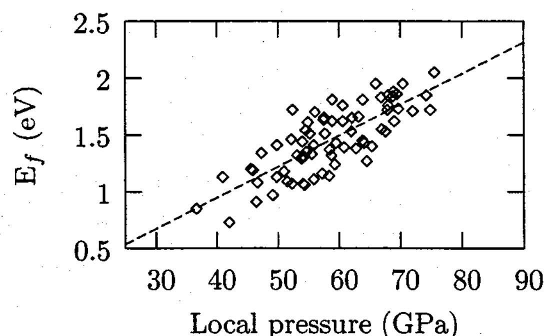

FIG. 10. Oxygen interstitial formation energies versus the initial local stress. The correlation coefficient for the linear regression is 0.84.

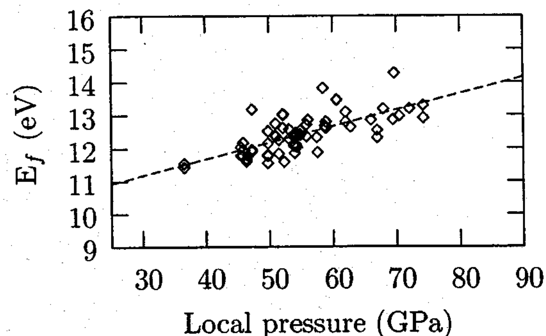

FIG. 12. Silicon interstitial formation energies versus the initial local stress. The correlation coefficient for the linear regression is 0.67.

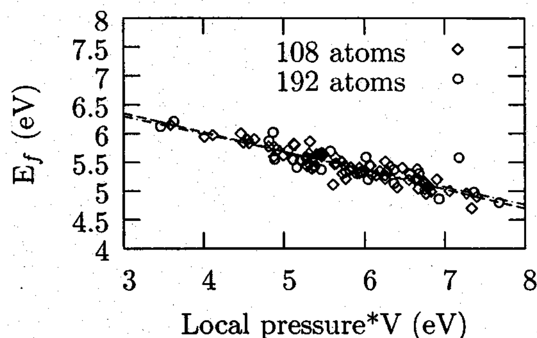

FIG. 13. Oxygen vacancy formation energies versus the initial local pressure for the 108-atom and 192-atom supercells, where V is the mean atomic volume. The correlation coefficient for the linear regression of the 192-atom system is 0.84.

dard deviation of 0.30, the same values for the average formation energy and standard deviation as those for the 108-atom silica (see Sec. V A). The point to point mean error between the two linear regression (108 atoms and 192 atoms) is 0.03 eV.

As far as oxygen vacancies are concerned, and considering the errors of the model, the 108-atom silica supercell seems large enough for a good description of the mean defect formation energy and its fluctuations. We expect that this is also the case for oxygen interstitials which also show a close correlation between local stress and formation energies.

The stress dispersion in an even larger system, 648 atoms, is also in perfect agreement with this conclusion. The extrapolated mean formation energy is found to be 5.40 eV with a standard deviation of 0.26 eV.

C. Comparison with diffusion experiments

A comparison of our results with experiments cannot be done directly. Indeed, the only information on defect formation energy values comes from the measure of activation energies in diffusion experiments. Furthermore, looking at the results, the average migration barriers of neutral oxygen defects have to be close to the migration barriers found in α-quartz.[8] We already have shown that for oxygen defects the structures and formation energies are similar to those of quartz and that this similarity comes from their very local character. We have already calculated some migration barriers for oxygen defects and these preliminary results are close in energy and in migration path to the quartz results. In the homogeneous regime, where silica is in equilibrium with itself, the activation energy for the network oxygen migration is therefore expected to be about 4.6 eV, taking into account half of the mean formation energy of a Frenkel pair in silica glass and the interstitial migration barrier in quarz of 1.2 eV.[8] Using our preliminary results pointing to a migration barrier of 1.4 eV, we find an activation energy of 4.8 eV. Both results are in good agreement with the experimental measurement[45] of 4.7 eV. This agreement strengthens our confidence in the predictive power of our calculations of formation energies. An exhaustive description of migration barriers will be the aim of a further study.

VII. CONCLUSION

In the context of the study of the long-term aging of silica glasses, we have performed a systematic study of neutral self-defects in a silica glass model by first principles. Combining empirical potential molecular dynamics and first-principles calculations we successfully adjusted a procedure allowing to obtain amorphous networks displaying a structure close to the experimental one, free of artefacts due to the numerical generation of the glass model itself and at a low CPU time cost.

In order to determine the whole distribution of defect formation energies and structures we needed a quick enough method for ground state calculations. We chose then a first-principles method where the wave functions are projected onto a localized pseudo–atomic orbital basis set. Reducing the number of basis vectors is a way to reduce the computational effort. Of course, the results had to be compared to other methods which do not suffer from the uncertainity due to the basis set choice. We have compared plane wave basis set codes (PWSCF and VASP) and a localized pseudo–atomic orbital basis set code (SIESTA), showing that both methods give the same results within an error that we attribute mainly to differences in the first-principles scheme. These differences result in small variations in silica formation energy, O_2 cohesion, and silicon bulk cohesion.

We have found that the defect formation energies and structures are distributed. In the case of oxygen defects (vacancies and interstitials), the formation energy distribution is mainly due to local distortions which may be quantified using the local stress. The relation between local stress and energy dispersion is linear according to Eq. (13). With this model, we show, by comparing the results for different silica sizes, that the 108-atom glass model is statistically representative, in terms of mean formation energy and formation energy fluctuations, of oxygen defects in a silica glass. In the case of silicon defects, as the induced displacements are important, the linear expansion is no longer valid. As discussed, the formation energy of silicon defects exhibits a stronger dependence on nonlocal properties than oxygen defects. A larger system is probably needed to take into account accurately the formation energy fluctuations. However, the 108-atom silica model gives a first insight into the variety and the energy scales of defect types. For instance, it is clearly shown that the average formation energy of silicon defects in a silica glass is definitively lower than in quartz.

Concerning the comparison with diffusion experiments, our first migration results are in good agreement with the experimental migration activation energy for intrinsic oxygen.

ACKNOWLEDGMENTS

We wish to acknowledge all the collaborators from the laboratory, with special thanks to Professor M. Heritier (Paris XI) for his support and to J. Dalla Torre whose vision of atomic stress was a source of inspiration.[46]

*Present address: Service de Recherche en Métallurgie Physique, CEA-Saclay, 91191 Gif-sur-Yvette, France.

[1] L. Martin-Samos, Y. Limoge, N. Richard, J.-P. Crocombette, G. Roma, E. Anglada, and E. Artacho, Europhys. Lett. **66**, 680 (2004).
[2] D. C. Allan and M. P. Teter, J. Am. Ceram. Soc. **73**, 3247 (1990).
[3] K. C. Snyder and W. Fowler, Phys. Rev. B **48**, 13238 (1993).
[4] C. M. Carbonaro, V. Fiorentini, and S. Massidda, J. Non-Cryst. Solids **221**, 89 (1997).
[5] D. R. Hamann, Phys. Rev. Lett. **81**, 3447 (1998).
[6] N. Capron, S. Carniato, A. Lagraa, G. Boureau, and A. Pasturel, J. Chem. Phys. **112**, 9543 (2000).
[7] A. Pasquarello, Appl. Surf. Sci. **166**, 451 (2000).
[8] G. Roma, Y. Limoge, and S. Baroni, Phys. Rev. Lett. **86**, 4564 (2001).
[9] A. M. Stoneham, M. A. Szymanski, and A. L. Shluger, Phys. Rev. B **63**, 241304 (2001).
[10] Z.-Y. Lu, C. J. Nicklaw, D. M. Fleetwood, R. D. Schrimpf, and S. T. Pantelides, Phys. Rev. Lett. **89**, 285505 (2002).
[11] J. R. Chelikowsky, D. J. Chadi, and N. Binggeli, Phys. Rev. B **62**, R2251 (2000).
[12] M. A. Lamkin, F. L. Riley, and R. J. Fordham, J. Eur. Ceram. Soc. **10**, 347 (1992).
[13] A. Bongiorno and A. Pasquarello, Phys. Rev. Lett. **88**, 125901 (2002).
[14] G. Roma and Y. Limoge, Nucl. Instrum. Methods Phys. Res. B **202**, 120 (2003).
[15] G. Roma and Y. Limoge, Phys. Rev. B **70**, 174101 (2004).
[16] P. Ordejón, E. Artacho, and J. M. Soler, Phys. Rev. B **53**, R10441 (1996).
[17] J. M. Soler, E. Artacho, J. D. Gale, J. J. A. García, P. Ordejón, and D. Sánchez-Portal, J. Phys.: Condens. Matter **14**, 2745 (2002).
[18] M. Benoit, S. Ispas, P. Jund, and R. Jullien, Eur. Phys. J. B **13**, 631 (2000).
[19] B. W. H. van Beest, G. J. Kramer, and R. A. van Santen, Phys. Rev. Lett. **64**, 1955 (1990).
[20] K. Vollmayr, W. Kob, and K. Binder, Phys. Rev. B **54**, 15808 (1996).
[21] P. Vashishta, R. Kalia, and J. P. Rino, Phys. Rev. B **41**, 12197 (1990).
[22] J. P. Rino, I. Ebbsjo, R. K. Kalia, A. Nakano, and P. Vashishta, Phys. Rev. B **47**, 3053 (1993).
[23] S. V. King, Nature (London) **47**, 3053 (1967).
[24] C. S. Marians and L. W. Hobbs, J. Non-Cryst. Solids **119**, 269 (1990).
[25] C. S. Marians and L. W. Hobbs, J. Non-Cryst. Solids **124**, 242 (1990).
[26] K. Goetzke and H.-J. Klein, J. Non-Cryst. Solids **127**, 215 (1991).
[27] L. W. Hobbs, C. E. Jesurum, V. Pulim, and B. Berger, Philos. Mag. A **78**, 679 (1998).
[28] X. Yuan and A. Cormack, Comput. Mater. Sci. **24**, 343 (2002).
[29] J. M. Nedelec and L. L. Hench, J. Non-Cryst. Solids **255**, 163 (1999).
[30] L. van Brutzel, Ph.D. thesis, Univ. Paris VI, France,, 2000.
[31] J. R. G. D. Silva, D. G. Pinatti, C. E. Anderson, and M. L. Rudee, Philos. Mag. **31**, 713 (1975).
[32] P. G. Coombs, J. F. D. Natale, P. J. Hood, E. K. McElfresh, R. S. Wortman, and J. F. Schackelford, Philos. Mag. Lett. **51**, L39 (1985).
[33] R. L. Mozzi and B. E. Warren, J. Appl. Crystallogr. **2**, 164 (1969).
[34] E. Anglada, J. M. Soler, J. Junquera, and E. Artacho, Phys. Rev. B **66**, 205101 (2001).
[35] S. Baroni, A. D. Corso, S. de Gironcoli, and P. Giannozzi, http://www.PWSCF.org
[36] G. Kresse and J. Hafner, Phys. Rev. B **47**, RC558 (1993).
[37] G. Kresse and J. Furthmuller, Phys. Rev. B **54**, 11169 (1996).
[38] G. Kresse and J. Joubert, Phys. Rev. B **59**, 1758 (1999).
[39] J. Hardy, J. Phys. Chem. Solids **29**, 2009 (1968).
[40] H. Schober and K. Ingle, Philos. Mag. A **59**, 575 (1980).
[41] M. Gillan, Philos. Mag. A **48**, 903 (1983).
[42] V. Vitek and T. Egami, Phys. Status Solidi B **144**, 145 (1987).
[43] N. Chetty and R. M. Martin, Phys. Rev. B **45**, 6074 (1992).
[44] O. H. Nielsen and R. M. Martin, Phys. Rev. B **32**, 3780 (1985).
[45] J. C. Mikkelsen, Appl. Phys. Lett. **45**, 1187 (1984).
[46] J. Dalla Torre, J.-L. Bocquet, Y. Limoge, J.-P. Crocombette, E. Adam, G. Martin, T. Baron, P. Rivallin, and P. Mur, J. Appl. Phys. **92**, 1084 (2002).
[47] A ring is a closed path.
[48] An n-membered ring is a closed path formed by n units. In the SiO_2 case the units are SiO_4 tetrahedra.